



Article

Design and Characterization of an Adjustable Passive Flow Regulator and Application to External CSF Drainage

Eric Chappel

Microsystems Department, Debiotech SA, 1004 Lausanne, Switzerland; e.chappel@debiotech.com

Abstract: Passive valves that deliver a constant flow rate regardless of inlet pressure changes have numerous applications in research, industry, and medical fields. The present article describes a passive spring valve that can be adjusted manually to deliver the required flow rate. The valve consists of a movable rod with an engraved microchannel. The fluidic resistance of the device varies together with the inlet pressure to regulate the flow rate. A prototype was made and characterized. Flow-rate adjustment up to $\pm 30\%$ of the nominal flow rate was shown. A simple numerical model of the fluid flow through the device was made to adapt the design to external ventricular drainage of cerebrospinal fluid (CSF). Some insights about the implementation of this solution are also discussed.

Keywords: passive valve; flow control; constant flow regulator; external ventricular drain (EVD); cerebrospinal fluid (CSF)

1. Introduction

Passive flow regulators or flow-controlled valves deliver a constant flow rate regardless of pressure variations [1]. These compact, reliable, maintainable and energy-free valves are widely used in industry for many applications, including water treatment, process water control, centrifugal pump protection, water-saving, irrigation, etc. [2,3]. These passive valves usually have moving parts, and automatic adjustment of flow to pressure conditions is achieved by changing the dimensions of the fluid path. A variation of pressure moves a flexible element of the device to induce a change in the fluidic path cross-section or length. The flexible element can be a silicon membrane [4–13], an elastomeric membrane [14–23], a silicone tube [24], a thin flap [25–28], or a moving piston [29,30].

Several implantable passive flow-controlled valves have been considered for the drainage of cerebrospinal fluid (CSF) from the brain ventricles toward the peritoneum cavity for the treatment of hydrocephalus [7,13,22–24,29,31–33]. The single flow-control valve available on the market is the OSVII™ (Integra Life Science, Princeton, NJ, USA). Two models are proposed, covering the following ranges of flow rate: 8 to 17 mL/h, to meet the special needs of normal-pressure hydrocephalus (NPH) patients requiring a lower flow rate, and 18 to 30 mL/h [23]. This three-stage passive flow-regulated valve has a flexible silicone membrane with a narrow orifice surrounding a pin of changing diameter. In the first stage, also called the differential pressure stage, the valve operates as a standard differential pressure valve with low hydraulic resistance. In the flow-regulating stage, the membrane goes down and the pin progressively narrows the orifice to maintain the flow constant. The third stage is reached under high-pressure conditions (above 36 mbar). The membrane moves beyond the pin, and the hydraulic resistance is thus considerably reduced. This technology, introduced in 1987 by Cordis, was included in many shunt evaluation campaigns [1,22,34]. In principle, this flow-regulating shunt should limit the risk of overdrainage associated with differential shunts but, in turn, may induce excessive CSF pressure during cerebrovascular fluctuations in patients with limited pressure–volume compensatory reserve [34]. An alternative to account for individual-to-individual variability in CSF production rate and cerebrovascular fluctuations is the implementation of the



Citation: Chappel, E. Design and Characterization of an Adjustable Passive Flow Regulator and Application to External CSF Drainage. *Micromachines* **2023**, *14*, 675. <https://doi.org/10.3390/mi14030675>

Academic Editor: Kwang-Yong Kim

Received: 10 January 2023

Revised: 6 March 2023

Accepted: 17 March 2023

Published: 19 March 2023



Copyright: © 2023 by the author. Licensee MDPI, Basel, Switzerland. This article is an open access article distributed under the terms and conditions of the Creative Commons Attribution (CC BY) license (<https://creativecommons.org/licenses/by/4.0/>).

specific fluidic profile that should allow better control of intracranial pressure (ICP) [32]. A MEMS-based passive flow-regulating valve has been designed to evaluate this solution [13]. The device consists of a flexible membrane with holes and facing pillars that form valves that close progressively as the pressure increases. The resulting reduction of the gap between the membrane and the pillars leads to an increase in hydrodynamic resistance. Numerical simulations have been performed to obtain the targeted flow profile. MEMS technology offers numerous advantages in terms of manufacturing cost, repeatability, and reliability, but the small dimensions of the fluid pathway make the device sensitive to contamination and prone to clogging [13].

The external ventricular drainage (EVD) of CSF is commonly used in intensive care units in patients with elevated ICP. This condition may be associated with tumors, hemorrhage, aneurysm, meningitis, traumatic brain injury, acute obstructive hydrocephalus, etc. Standard external drainage systems consist of a set of different elements fixed to an intravenous (IV) pole, including catheter and fluidic lines, stopcocks, a burette to monitor the flow rate, access ports (for priming, sampling, purging, etc.), a pressure sensor, a check valve (e.g., duckbill valve), a collecting bag and a means to adjust the position of the burette and level the system with the tragus. The fluidic lines exhibit a small fluidic resistance, thus misuse, the patient's movements, etc., without clamping of the line can lead to severe overdrainage potentially causing patient death [35]. A flow-control valve is, by design, more robust to misuse and modifications of the fluidic line position. The challenge here is to provide a device compatible with a large range of potential CSF flow rates (which is unknown at the beginning of the treatment). In addition, the weaning procedure at the end of the treatment requires a progressive reduction of the flow through the valve. Finally, because the fluid to be drained is often hemorrhagic, the design of the valve should exhibit a good tolerance to contamination, with ideally a purge mode.

A flow-control valve with adjustable means and a purge mode is therefore desirable for this specific application (EVD). The focus here is on the original design of an adjustable passive valve for insertion into the fluid path of a standard external drainage system. Valve setting is also an important feature of other potential applications, such as pain management, where the delivery rate is tailored to patient experience. To date, the only adjustable passive valve is a MEMS microvalve, in which the fluid path is adjusted manually or passively adjusted to deliver a constant flow, regardless of viscosity changes due to temperature variation [36]. However, this device is not suitable for EVD, due to its sensitivity to contamination [13].

The spring valve design that was considered for the internal diversion of CSF from the brain ventricles to the peritoneal cavity [29] was adapted to allow manual adjustment of the flow rate. Indeed, this valve technology offers several competitive advantages that make it an interesting candidate for such a feasibility study. First, the device has relatively large fluid openings that would limit the risk of clogging. In addition, the valve has self-cleaning capabilities and can be easily purged [1,29]. This modular valve is compatible with the standard turning process and therefore compatible with the low cost requirements of a fully disposable EVD system. Finally, adjustability can be obtained in a relatively simple manner as the nonlinearity of the flow profile is obtained with a linear element (the compression spring). Other flow-adjustment features have been theoretically proposed for a MEMS-based valve, but this solution would require a complex and difficult assembly process [33]. The original valve consists of a moving cylinder with a spiral groove and a linear compression spring inside a hollow cylinder with openings (see Figure 1). At rest, the piston is partly engaged into the narrow part of the cylinder. As the pressure force on the piston increases, the piston is engaged further into the cylinder and the fluid is forced to flow through a longer channel length. The force generated by the spring increases linearly with the applied pressure and thus the movement of the piston leads to a linear increase in the channel length as the pressure increases. As the channel cross-section and spiral pitch are constant, the flow is regulated at a predetermined fixed value. At high pressure, the device can either exhibit free flow or an occlusion state.

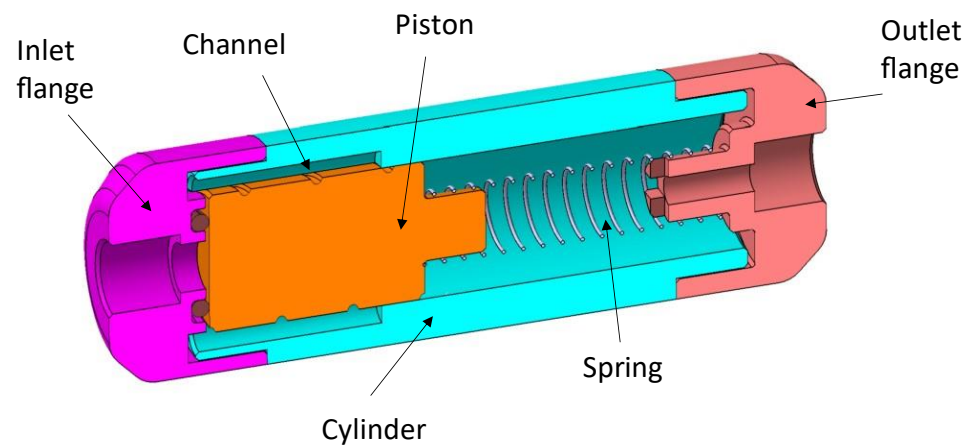


Figure 1. Cross-section of the passive constant flow valve at rest. The piston is engaged in the narrow part of the cylinder. Increasing the pressure leads to a movement of the piston to the right until the pressure force onto the piston is balanced by the spring restoring force. The fluid is forced to flow through the channel engraved into the piston.

In the present study, the means to manually adjust the flow rate was analyzed through modeling and experimentation. The fluidic model was presented first followed by a description of the prototypes and the fluidic characterizations. Finally, simulations are shown of an adjustable spring valve design dedicated to EVD.

2. Materials and Methods

2.1. Modeling

2.1.1. Simplified Model

The simplified model does not consider the effect of gravity and the singular head losses along the fluid path. The different notations used to model the fluidic behavior of the device are illustrated in Figure 2.

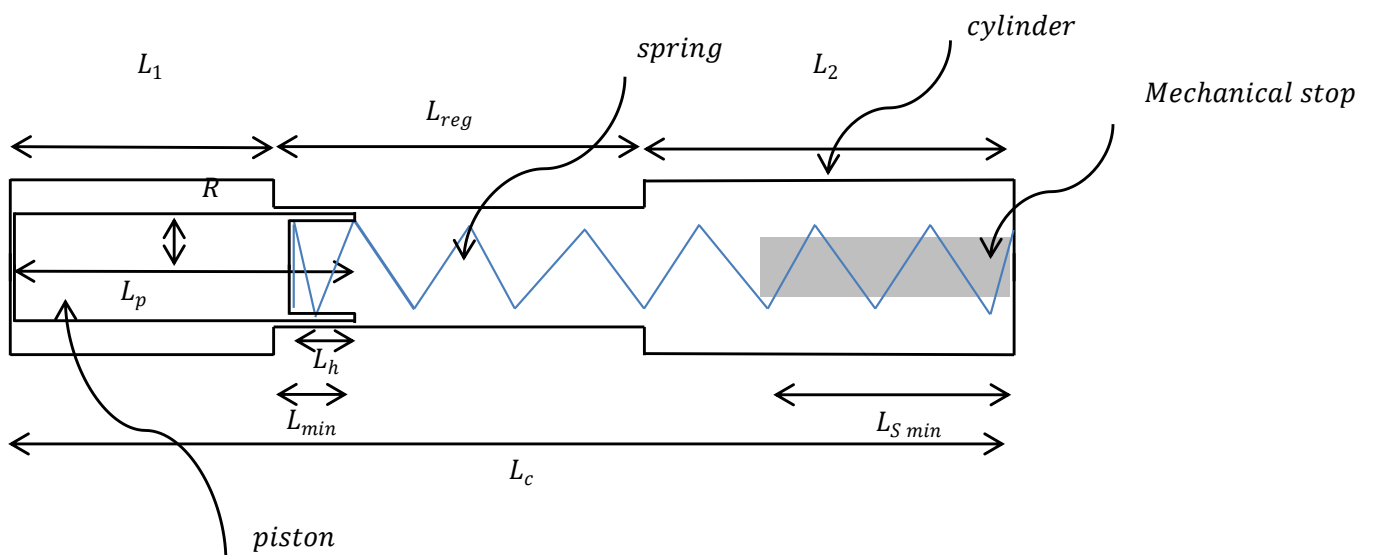


Figure 2. Schematic cross-section of the adjustable flow-control valve. The notations are described in the nomenclature.

According to [29], the length L_{loop} of one loop of the helicoidal channel is:

$$L_{loop} = 2\pi \sqrt{\left(R - \frac{D_h}{2}\right)^2 + b^2} \quad (1)$$

where R is the piston radius, $2\pi b$ the helix pitch, and D_h the hydraulic diameter of the channel.

Consequently, the channel length per unit of piston length α takes the form:

$$\alpha = \frac{L_{loop}}{2\pi b} = \sqrt{1 + \left(\frac{R - \frac{D_h}{2}}{b}\right)^2} \quad (2)$$

The channel cross-section is depicted in Figure 3, wherein the opening angle of the channel is noted θ and the radius of curvature R . The flow of the incompressible medium is assumed to be laminar with negligible singular losses.

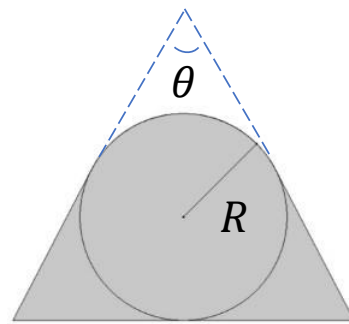


Figure 3. Schematic cross-section (in light grey) of the piston channel with a radius of curvature R at the bottom of the channel. θ is the opening angle.

The fluidic resistance β of the channel per unit of length, according to the Darcy-Weisbach equation [37], is, in agreement with [29]:

$$\beta = \frac{32\eta}{D_h^2 \cdot Area} = \frac{256\eta}{D_h^4 \left(\pi - \theta + 4 \left(\tan \frac{\theta}{2} + \frac{1}{\cos \frac{\theta}{2}} \right) \right)} \quad (3)$$

where D_h is the hydraulic diameter defined as:

$$D_h = 4 \frac{Area}{Wetted\ perimeter} = 2R \quad (4)$$

Several assumptions are made to estimate the position of the piston at different values of the applied pressure:

- $L_{min} = L_p - L_1 > 0$ (i.e., there is no free flow at low pressure).
- the channel cross-section is regular.
- the spring stiffness k is constant (i.e., independent from the compression).
- $\Delta L_{S0} = L_{min}$ (the condition for a constant flow rate).
- $R \gg D_h$ (the effective surface for pressure force calculation is not affected by the channel).
- $L_c = L_{reg}$ (to simplify the numeral modeling).

The effective channel entrance is neglected if the hydraulic diameter is much smaller than the channel length. The effective channel length, considering the correction due to the geometry at the inlet and outlet of the channel, is, for $D_h \ll L_{ch}$:

$$L_{ch\ eff} = L_{ch} - \frac{D_h}{\tan(\theta)} = L_{ch} - D_h \frac{L_{loop}}{pitch} = L_{ch} - \alpha D_h \approx L_{ch} \quad (5)$$

According to [1], the fluidic characteristic of a flow regulator can be split into three different stages, as illustrated in Figure 4:

- Stage I—low-pressure stage
- Stage II—flow-regulation stage
- Stage III—high pressure

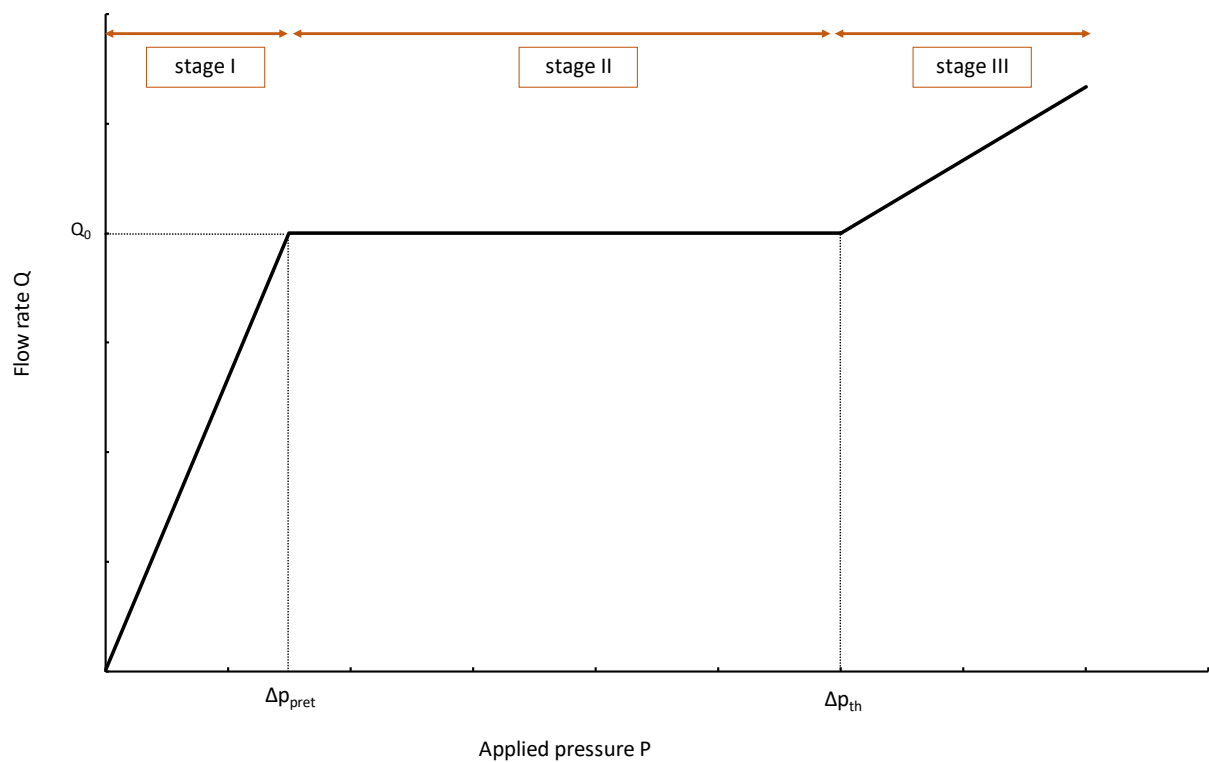


Figure 4. Ideal flow rate versus pressure gradient characteristic of a three-stage passive constant flow regulator. At low pressure (Stage I), the regulator has a constant and low hydraulic resistance. In Stage II, the flow is regulated at Q_0 for a pressure gradient in the range $[\Delta P_{pret}; \Delta P_{th}]$. At high pressure (Stage III), the device delivers a large flow rate.

Stage I

The minimum pressure (or pretension) P_{pret} to move the piston is:

$$P_{pret} = \frac{k \Delta L_{S0}}{S} = \frac{k L_{min}}{S} \quad (6)$$

If $P < P_{pret}$ and the outlet groove length $L_2 = 0$, then the piston displacement ΔL is equal to zero and the fluidic resistance is constant:

$$\begin{cases} \Delta L = 0 \\ Rf_0 = \alpha \beta L_{min} = Cte \end{cases} \quad (7)$$

Thus, the flow rate in Stage I varies linearly with the pressure:

$$Q(P < P_{pret}) = \frac{P}{R_{f0}} = \frac{P}{\alpha\beta L_{min}} \quad (8)$$

and reaches, at $P = P_{pret}$:

$$Q(P = P_{pret}) = \frac{P_{pret}}{R_{f0}} = \frac{P_{pret}}{\alpha\beta L_{min}} = \frac{k}{\alpha\beta S} \quad (9)$$

Stage II

If $P_{pret} < P < P_{th}$, the piston displacement and the fluidic resistance become:

$$\begin{cases} \Delta L = \frac{S(P - P_{pret})}{k} \\ R_f = \alpha\beta(L_{min} + \Delta L) = \alpha\beta\left(L_{min} + \frac{S(P - P_{pret})}{k}\right) \end{cases} \quad (10)$$

The fluidic resistance varies with the applied pressure to compensate for the pressure variation. The flow rate Q in Stage II is therefore:

$$Q(P_{pret} < P < P_{th}) = \frac{P}{\frac{P_{pret}}{Q(P=P_{pret})} + \alpha\beta\frac{S(P-P_{pret})}{k}} = \frac{P}{\frac{P_{pret}}{Q(P=P_{pret})} + \frac{(P-P_{pret})}{Q(P=P_{pret})}} \quad (11)$$

which simplifies into:

$$(P_{pret} < P < P_{th}) = Q(P = P_{pret}) = \frac{k}{\alpha\beta S} = Cte \quad (12)$$

According to the above hypothesis, the flow in Stage II is unaffected by pressure variations.

Stage III

At higher pressures, for $P > P_{th}$, and considering that there are no openings in the cylinder:

$$\begin{cases} \Delta L_{th} = \frac{S(P_{th} - P_{pret})}{k} \\ R_f = \alpha\beta(L_{min} + \Delta L_{th}) = Cte \end{cases} \quad (13)$$

The fluidic resistance is constant again and the flow rate increases with the applied pressure:

$$Q(P > P_{th}) = \frac{P}{\alpha\beta(L_{min} + \Delta L_{th})} \quad (14)$$

In the presence of cylinder openings of length L_2 (see Figure 2), the part of the piston channel engaged into the narrowest part of the cylinder, after having reached a maximum, is reduced at high pressure. This part of the piston that is fluidically active is equal to:

$$\Delta L + L_{min} \text{ if } 0 < \Delta L < L_{reg} - L_{min} \quad (15)$$

Or

$$L_p - \Delta L + L_{reg} - L_{min} \text{ if } \Delta L \geq L_{reg} - L_{min} \quad (16)$$

Free flow conditions can be obtained at high pressure if the medium can bypass the channel and directly flow through to the openings of the cylinder that have very small fluidic restrictions.

2.1.2. Non-Uniform Channel

If the channel is not uniform and if $L_2 \neq 0$, special care should be taken to derive the fluidic resistance of the channel as a function of the pressure.

We consider for instance a piston wherein the hydraulic diameter is not constant along the helix: the initial part of the piston (length L_{min}) that is engaged in the narrowest part of the cylinder is characterized by the coefficients α_1 and β_1 while the other part of the piston (length $L_p - L_{min}$) is characterized by α_2 and β_2 .

If $0 \leq \Delta L \leq L_{reg} - L_{min}$ and $L_p \geq L_{reg}$, the fluidic resistance of the channel is now:

$$R_f = \alpha_1 \beta_1 L_{min} + \alpha_2 \beta_2 \Delta L = \alpha_1 \beta_1 L_{min} + \alpha_2 \beta_2 \frac{S(P - P_{pret})}{k} \quad (17)$$

The flow rate in Stage II takes the form:

$$Q = \frac{P}{\alpha_1 \beta_1 L_{min} + \alpha_2 \beta_2 \frac{S(P - P_{pret})}{k}} = \frac{P}{\frac{P_{pret}}{Q(P = P_{pret})} + \frac{\alpha_2 \beta_2}{\alpha_1 \beta_1} \times \frac{(P - P_{pret})}{Q(P = P_{pret})}} \quad (18)$$

Finally,

$$\frac{Q}{Q(P = P_{pret})} = \frac{P}{P_{pret}} \times \frac{1}{1 + \frac{\alpha_2 \beta_2}{\alpha_1 \beta_1} \left(\frac{P}{P_{pret}} - 1 \right)} \quad (19)$$

For $\alpha_1 \beta_1 \neq \alpha_2 \beta_2$ the flow rate profile is no longer flat as increases of the inlet pressure.

If $L_{reg} - L_{min} \leq \Delta L \leq L_{reg}$ and $L_p \geq L_{reg} + L_{min}$ the flow rate can be estimated using the following formulation of the fluidic resistance:

$$R_f = \alpha_1 \beta_1 (L_{reg} - \Delta L) + \alpha_2 \beta_2 \Delta L = \alpha_1 \beta_1 L_{reg} - \Delta L (\alpha_1 \beta_1 - \alpha_2 \beta_2) \quad (20)$$

These formulae are useful to obtain a specific regulation profile. Depending on the complexity of the target profile, modulation of the channel pitch or change in the channel cross-section can be considered.

2.1.3. Gravity Effect and Device Orientation

The weight of the piston is an additional force that should be considered to refine the model. The angle between the horizontal axis and the piston axis is noted as φ . The effective weight of the piston (after correction due to Archimedes' force) is noted as m . The minimum applied pressure to move the piston becomes:

$$P_{pret} = \frac{k L_{min} - mg \sin \varphi}{S} \quad (21)$$

The flow rate at $P = P_{pret}$ is, therefore:

$$Q(P = P_{pret}) = \frac{P_{pret}}{R_{f0}} = \frac{k L_{min} - mg \sin \varphi}{\alpha \beta S L_{min}} = \frac{k}{\alpha \beta S} - \frac{mg \sin \varphi}{\alpha \beta S L_{min}} \quad (22)$$

In Stage II, for $P_{pret} < P < P_{th}$, the piston displacement and the fluidic resistance are:

$$\begin{cases} \Delta L = \frac{S(P - P_{pret})}{k} \\ R_f = \alpha \beta (L_{min} + \Delta L) = \alpha \beta \left(L_{min} + \frac{S(P - P_{pret})}{k} \right) \end{cases} \quad (23)$$

The corresponding flow rate is:

$$\begin{aligned} Q(P_{pret} < P < P_{th}) &= \frac{P}{\frac{P_{pret}}{Q(P=P_{pret})} + \alpha \beta \frac{S(P-P_{pret})}{k}} \\ &= \frac{P}{\frac{P_{pret}}{Q(P=P_{pret})} + \frac{(P-P_{pret})}{Q(P=P_{pret}) \left(1 + \frac{mg \sin \varphi}{S P_{pret}}\right)}} \neq Cte \end{aligned} \quad (24)$$

The flow rate is not perfectly constant if the effective mass of the piston cannot be neglected.

2.1.4. Out-of-Channel Flow

The difference in diameter between the cylinder and the piston induces a leakage between the loops of the channel. It is assumed that this parasitic flow is proportional to the active height of the piston equal to $\frac{L_{ch\ eff}}{\alpha}$ and normal to the channel flow. This leakage is considered effective outside of the channel over a distance equal to:

$$\frac{L_{ch\ eff}}{\alpha} \times \left(1 - \frac{w_{ch}}{2\pi b}\right) = \frac{L_{ch\ eff}}{L_{loop}} \times (2\pi b - w_{ch}) \quad (25)$$

where w_{ch} is the channel width. In a first approximation, the piston and the cylinder are concentric and thus the fluidic resistance of the parasitic flow per unit of length is [38]:

$$R_{f\ losses}/L = \frac{8\eta}{\pi \left(R_c^4 - R^4 - \frac{(R_c^2 - R^2)^2}{\ln \frac{R_c}{R}} \right)} \quad (26)$$

The total parasitic fluidic resistance is parallel to the channel flow is, therefore:

$$R_{f\ losses} = \frac{8\eta}{\pi \left(R_c^4 - R^4 - \frac{(R_c^2 - R^2)^2}{\ln \frac{R_c}{R}} \right)} \times \frac{L_{ch\ eff}}{L_{loop}} \times (2\pi b - w_{ch}) \quad (27)$$

The combination of both resistances in parallel leads to the global fluidic resistance equal to:

$$R_f = \frac{R_{f\ ch} \times R_{f\ losses}}{R_{f\ ch} + R_{f\ losses}} \quad (28)$$

where $R_{f\ ch}$ is the fluidic resistance of the channel.

2.1.5. Other Fluid Restrictions

The fluidic line exhibits a fluidic resistance $R_{f\ line}$. If this resistance is not negligible, this additional pressure drop shall be considered. For a given pressure gradient in the valve ΔP_{valve} , the flow rate Q is calculated according to the model described hereabove.

The additional pressure drop ΔP_{line} due to $R_{f\ line}$ is:

$$\Delta P_{line} = R_{f\ line} Q \quad (29)$$

The effective pressure gradient that generates the flow rate Q is:

$$\Delta P_{eff} = \Delta P_{valve} + \Delta P_{line} \quad (30)$$

It is noteworthy that the resulting curve may exhibit points that cannot be obtained experimentally (see for instance the curve obtained at 60 mm (Sim60) in Figure 10 as well as the discussion about hysteresis).

An alternative method consists of directly solving the flow equation.

It is first assumed that the pressure gradient along the channel is larger than P_{pret} . Thus,

$$\Delta P_{eff} = \Delta P_{valve} + \Delta P_{line} = \left(R_{f0} + R_{f\ line} + \gamma \left(\Delta P_{eff} - R_{f\ line} Q - P_{pret} \right) \right) Q \quad (31)$$

where $\gamma = \frac{\alpha \beta S}{k}$.

The resulting flow equation is:

$$\gamma R_{f\ line} Q^2 - \left(R_{f0} + R_{f\ line} + \gamma \left(\Delta P_{eff} - P_{pret} \right) \right) Q + P = 0 \quad (32)$$

With general solutions of the form:

$$Q = \frac{\varphi \pm \sqrt{\varphi^2 - 4\gamma R_{f\ line} \Delta P_{eff}}}{2\gamma R_{f\ line}} \quad (33)$$

with

$$\varphi = R_{f0} + R_{f\ line} + \gamma \left(\Delta P_{eff} - P_{pret} \right) \quad (34)$$

The first hypothesis shall be verified using the estimated value of the flow rate.

- If $\Delta P_{eff} - R_{f\ line} Q - P_{pret} \leq 0$, then the flow is simply given by:

$$\Delta P_{eff} = \Delta P_{valve} + \Delta P_{line} = \left(R_{f0} + R_{f\ line} \right) Q \quad (35)$$

- If $\Delta P_{eff} - R_{f\ line} Q - P_{pret} > 0$, both solutions of Equation (33) are possible depending on the initial conditions (see the discussion about hysteresis).

2.2. Simulation

The model was coded and simulated using a visual programming language (LabVIEW, National Instruments). Each design parameter was introduced as a controller. Out-of-channel flow (leakage) is also considered as an option. The piston displacement and the flow rate are computed in the predefined inlet pressure range using constant pressure steps.

2.3. Prototyping

The prototype in stainless steel and PEEK (piston) was machined as illustrated in Figure 5, which shows the different elements of the passive adjustable flow regulator, respectively, the inlet flange, the piston and its spring, the cylinder, and the outlet flange. The assembly drawing is shown in Figure 6. The mechanical drawings of the sub-elements are provided in Appendix A (Figures A1–A4). The choice of materials and the external dimensions of the device were selected to obtain a prototype that is easy to machine and compatible with assembly and disassembly. The data obtained from metrology is indicated in parentheses. These values were used as input data for the numerical simulations. Since the piston is 2 mm shorter than expected, a 2 mm thick elastomeric disk was glue on the top of the cylinder to obtain the targeted spring preload and therefore limit the impact of this out-of-specs dimension onto the fluidic characteristic. Additionally, the clearance between the piston and the cylinder is larger than expected: the inner diameter of the cylinder is 18.035 mm instead of 18.015 mm. The spring dimensions and specifications are listed in Appendix B.



Figure 5. Prototype teardown showing, from left to right: the inlet flange, the piston, and the spring, the cylinder, and the outlet flange. Nominal dimensions are provided in the mechanical drawings. The height of the piston made of PEEK is 2 mm shorter than expected and the clearance between the piston and the cylinder is larger than expected (inner diameter of the cylinder at 18.035 mm instead of 18.015 mm); the other parts are within specification.

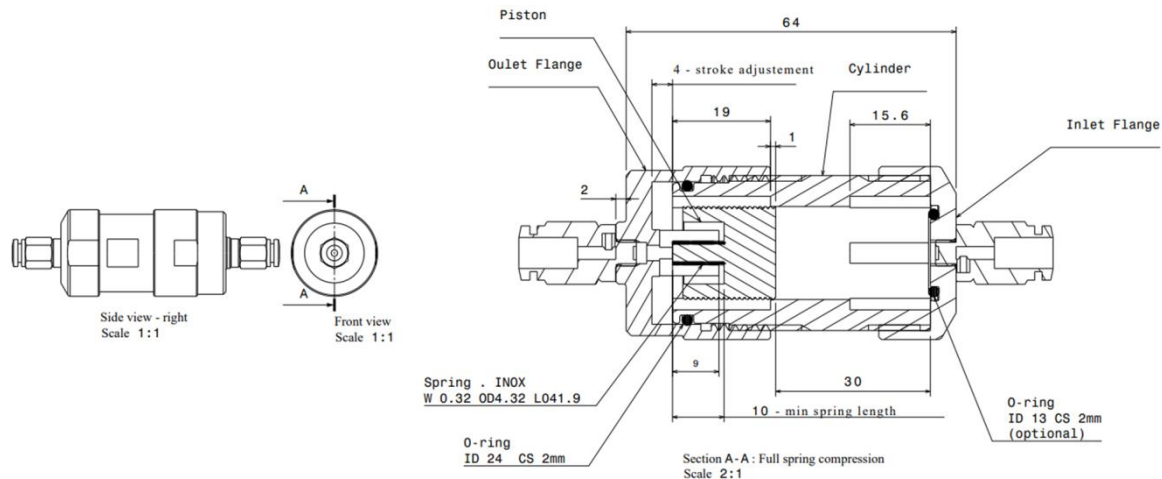


Figure 6. Side and front views of the device. The nominal dimensions are indicated in Section A-A.

2.4. Adjusting the Flow Rate

Several options can be considered to adjust the flow manually. The spring preload can be modified using the own weight m of the piston as illustrated in Figure 7.

For a rotation angle φ , the spring preload is equal to $mg \cos \varphi$, where $g = 9.81 \text{ m s}^{-2}$ is the gravitational acceleration. As illustrated in Figure 7, the predefined position of the rotating disk allows adjustment of the flow by gravimetry, the vertical position with the outlet above in the inlet corresponding to the higher flow rate.

The simplest method that was considered in this study consists of changing the spring preload with a rotating ring as illustrated schematically in Figure 8. The user turns the ring to modify the initial spring compression and therefore the fluidic characteristic of the device. Three different Positions 0, 1, and 2 were considered here, corresponding, respectively, to flange-to-flange distances of 64, 62, and 60 mm (see Figure 6 for Position 0 at 64 mm).

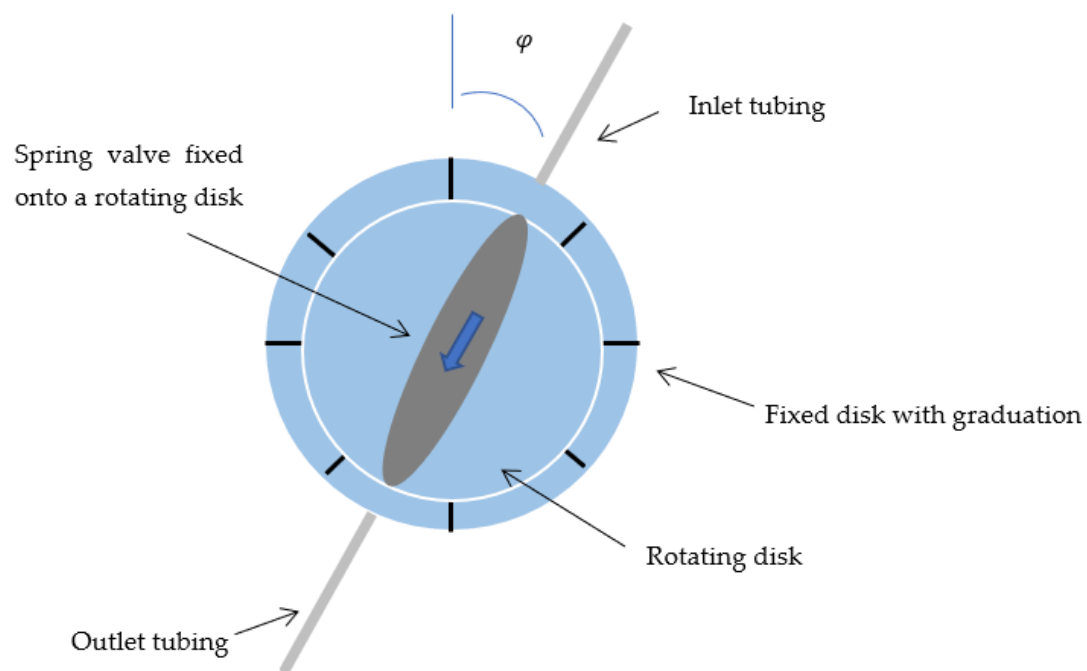


Figure 7. Spring valve mounted onto a rotation disk for gravimetric flow adjustment. The blue arrow indicates the direction of the flow. The rotation of the disk modifies the initial spring preload by gravimetry.

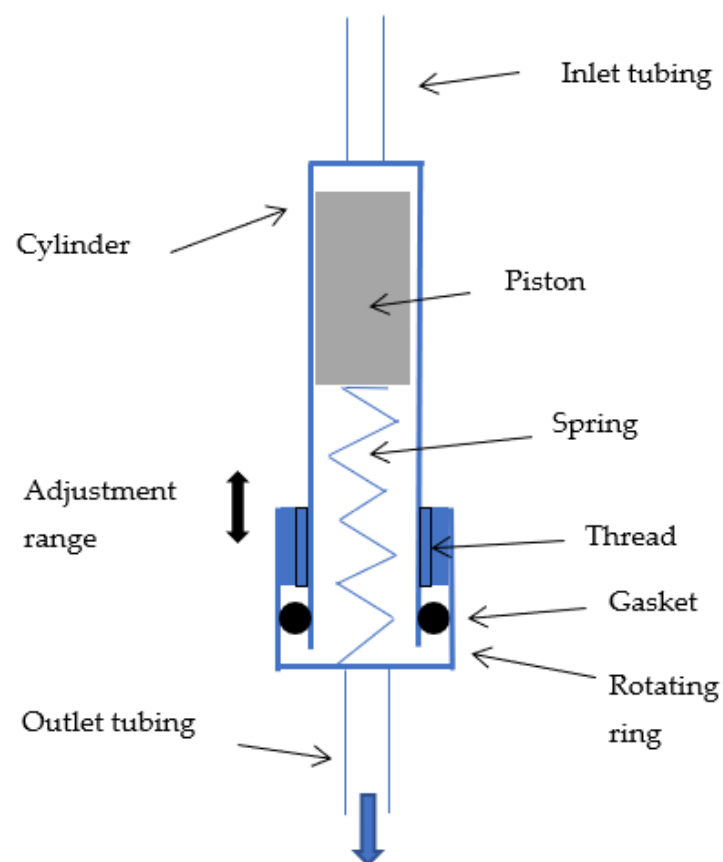


Figure 8. Adjustable flow-control spring valve with a rotating ring that allows the spring preload to be changed manually. A gasket between the ring and the cylinder is used to prevent leakage.

A more complex design includes a second colinear compression spring that becomes active either in a passive way at a given threshold pressure to increase the flow rate at high pressure, or actively by manual activation using a sliding sleeve that engages the second spring against the movable piston. According to [29], the valve at high flow could exhibit a free flow and become occlusive depending on the application and the need for a purge mode.

2.5. Adjusting the Pressure-Regulation Range

2.5.1. Regulation Threshold at Low Pressure

A rotating ring similar to the one described in Figure 8 is placed at the inlet of the device to adjust, using a shaft, the initial position of the piston and therefore the minimum value of the pressure-regulation range. As long as the spring is under compression, the shaft motion through the ring rotation induces a displacement of the piston.

2.5.2. Regulation Threshold at High Pressure

The maximum value of the pressure-regulation range is tuned through another shaft attached to the center of the ring. This shaft acts as a mechanical stop for the piston at high pressure. Rotating the ring induces a change in the spring maximum compression and thus a modification of the high-pressure part of the regulation range. The shaft should not be attached to the spring support to avoid any modification of the spring preload.

The different setting methods can of course be combined altogether in a single device. In this case, the shaft used to change the position of the mechanical stop limiting the motion of the piston at high pressure is mounted on the spring support ring through an additional ring.

2.6. Fluidic Characterization

Fluidic characterizations have been performed using water ISO 3 as the test medium. The test setup is shown in Figure 9.

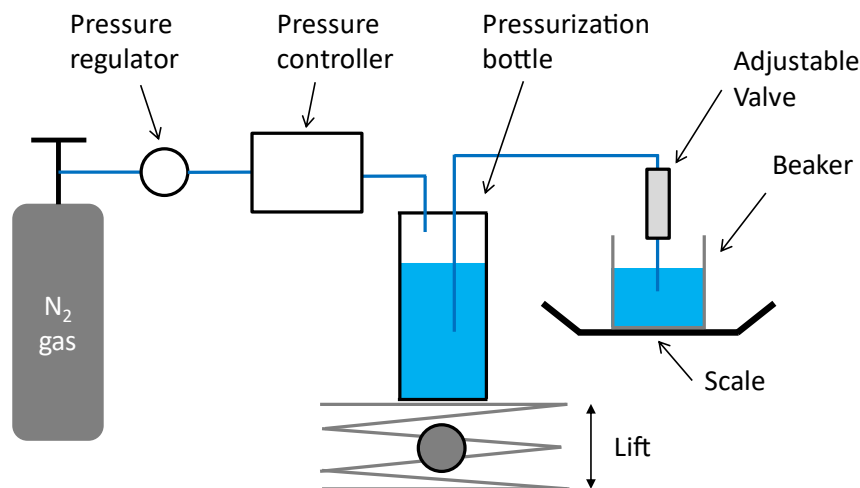


Figure 9. Schematic representation of the test setup.

The water is introduced into a pressurization bottle connected to a Druck DPI520 pressure controller. The fluid is forced to flow through the valve and is collected into a beaker placed onto a Sartorius MC1 LP620P scale. Pressure steps of 5 and 10 mbar have been used at low pressure. The typical stabilization time is 1 minute. The flow rate is estimated from weight measurements across 30 s, using a density of 1 g/mL at room temperature (20 °C). The valve is placed in the vertical position and tested using positive and negative steps of pressure.

As shown in Figure 9, special care has been taken to limit the water column of the fluidic line to less than 5 cm throughout the test. Three different settings of the valve have been tested, corresponding to a relative displacement of the outlet flange of 0 mm (Position 0), 2 mm (Position 1), and 4 mm (Position 2) from its nominal Position. The setting is controlled by a caliper that is used to measure the distance from the inlet to outlet flanges of, respectively, 64 mm, 62 mm, and 60 mm (see Figure 6).

3. Results

Experimental Results

The flow characteristics of the device at Positions 0 (64 mm), 1 (62 mm), and 2 (60 mm) are presented in Figure 10 and compared to simulations that consider the data obtained during the prototype metrology, out-of-channel flow, and the fluidic resistance of the fluidic line as well. The pressure-regulation range matches the theoretical expectations, considering a fluidic line resistance estimated experimentally to be about $4.3 \times 10^{10} \text{ Pa s/m}^3$.

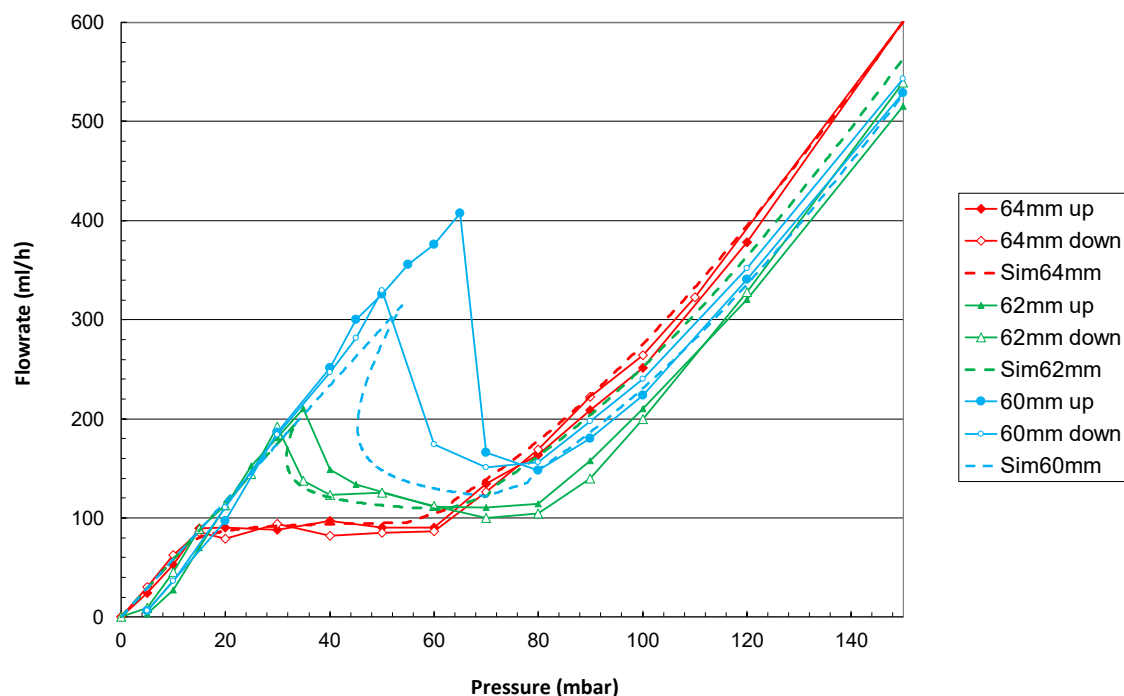


Figure 10. Flow rate versus pressure characteristics of the valve for the three different settings 0, 1, and 2 (corresponding to a flange-to-flange distance of, respectively, 64, 62, and 60 mm) using positive (up) and negative (down) pressure steps. The valve is tested vertically, with the inlet above the outlet. Dashed lines represent the numerical simulations of the valve for each setting.

Table 1 provides the pressure-regulation ranges and the mean flow rate for each setting. As expected, the increase of the spring preload by reducing the piston stroke induces an increase in the mean flow rate, since the piston requires more pressure force to initiate its movement. The match between the simulation and experiment is good at Positions 0 and 2. The fitting of the experimental data is more difficult at Position 3 because 3 hysteresis becomes important, and the regulation range is very narrow. In addition, simulated curves show a crossover point that cannot be measured experimentally, as discussed in Section 2.1.5.

Table 1. Regulation range and mean flow rate of the device at the three different settings.

	Position 0 (64 mm)		Position 1 (62 mm)		Position 2 (60 mm)	
	Experiment	Simulation	Experiment	Simulation	Experiment	Simulation
Regulation range (mbar)	[+15; +60]	[+15; +60]	[+30; +80]	[+40; +80]	[+60; +80]	[+52; +78]
Mean flow rate mL/h	91	92	120	114	160	130
St. dev. (%)	4	4	14	4	12	5.5

4. Discussion

4.1. Flow Regulation and Variability

The prototype was dimensioned to exhibit the nominal constant flow rate at the minimum spring preload (Position 0). As any change of the spring preload induces both a slope of the flow versus pressure characteristics together with a lowering of pressure-regulation range (see Figure 10 and Section 2.1), the design of a “flat” characteristic at an intermediate position is recommended, in order to explore both the positive and negative changes in the spring preload. Therefore, it is possible to obtain a flat profile across a wider range of settings. These results show that under constant temperature conditions, the flow rate can be adjusted up to at least $\pm 30\%$ by a simple rotation of the outlet flange by a few mm.

To maximize the channel cross-section and thus the tolerance to contamination, the prototype piston was designed with a very small spiral channel pitch. However, this also results in a high sensitivity to leakage out of the channel. Thus, the manufacturing capability must be considered when redesigning the system to limit the impact of machining tolerances on flow-rate variability. A compromise must be found between increasing the pitch and reducing the cross-sectional area of the channel and/or the piston diameter, which has an impact on sensitivity to contamination. An example of a design that has less sensitivity to manufacturing tolerances is provided in Section 4.3. Overall, flow regulation was achieved using a hydraulic diameter that is at least one order of magnitude larger than MEMS-based devices and other flow-controlled shunts [1,13,23]. Thus, this technology addresses one of the main concerns raised about using a flow-controlled valve for CSF drainage. The ability to flush the valve is also an attractive feature because the working fluid may be hemorrhagic. Finally, the adjustability enables the use of a single device for all patients with EVD and allows for a simplified weaning procedure.

4.2. Hysteresis

Hysteresis is intrinsically linked to the valve design and the additional fluidic resistance of the line. The flow characteristic obtained in Position 2 exhibits two different flow rates for a given pressure gradient within the range (45; 55) mbar. This phenomenon is due to the additional fluidic resistance of the line. As the applied pressure increases, the flow rate increases linearly as long as the piston remains in its initial position (no movement). Pressure drops are observed along the channel of the piston and the fluidic line itself. When the pressure gradient onto the piston surface is large enough to overcome the spring pretension, the piston moves to an equilibrium position.

At this given applied pressure P_1 , the fluidic resistance of the channel $R_{f\ ch}$ will increase as well as the whole resistance of the device equal to $R_{f\ ch} + R_{f\ line}$.

This results in a decrease in the flow rate Q

$$Q = \frac{P_1}{R_{f\ ch} + R_{f\ line}} \quad (36)$$

A lower flow rate requires a lower pressure at the inlet of the fluidic line with a constant fluidic resistance $R_{f\ line}$.

As the pressure reaches P_1 (the minimal applied pressure necessary to move the piston from rest), any increase in applied pressure will induce a lowering of the pressure downstream of the piston according to the mechanism described previously. This pressure lowering will induce an additional movement of the piston and progressively the piston will move until the system reaches an equilibrium position satisfying the flow equation described in Equation (32).

Without inlet pressure fluctuations, this forward movement of the piston begins at pressure:

$$P_{forward\ mov.} = P_{pret} \left(1 + \frac{R_{f\ line}}{R_{f0}} \right) \quad (37)$$

Conversely, when the piston is at a full stroke (high pressure) and considering negative pressure steps, the piston starts the backward movement at a pressure equal to:

$$P_{backward\ mov.} = P_{th} \left(1 + \frac{R_{f\ line}}{R_{f1}} \right) \quad (38)$$

where P_{th} is equal to the pressure gradient onto the piston that can push it against the stop limiter, R_{f1} being the fluidic resistance of the channel in this later position.

We infer that this hysteresis is notably a function of the parameters $R_{f\ line}$, R_{f0} , and R_{f1} .

This effect can be used to create an adjustable, automatic shut-off valve that prevents overflow in case of a sudden increase in the flow rate. This valve could be reversible or not (the piston can be blocked mechanically in a high position). On the other hand, hysteresis can be limited by limiting the pressure drops along the fluidic line.

4.3. Application to CSF Drainage

As the fluidic model shows a pretty good match with the experiment, new simulations were performed to adapt the current design to the flow and pressure range requirements of the CSF drainage.

The nominal flow rate was set at 20 mL/h at 37 °C, considering that CSF is equivalent to water in terms of viscosity [29]. The pressure-regulation range for an EVD can be set at 10 to 35 mbar or more. The design proposed in [29] for CSF drainage was chosen as a reference. The flow adjustment is obtained by changing the effective cylinder length with the rotating flange from 13.5 mm to 15.5 mm using steps of 0.5 mm, the nominal value being 14.5 mm. The simulated fluidic characteristics are shown in Figure 11, for a device in a horizontal position.

An interesting alternative method consists of using the piston weight and the orientation of the device to change the fluidic characteristic of the device. Figure 12 shows the simulation of a device described in [29], for two different orientations of the vertical piston (respectively, +90° with the inlet above the outlet and −90° with the outlet above the inlet), the effective weight of the piston here being equal to 500 mg. The device can be simply mounted onto a rotating disk with predefined positions, each position corresponding to a predetermined fluidic characteristic. The two methods can be combined to extend the range of accessible flow rates.

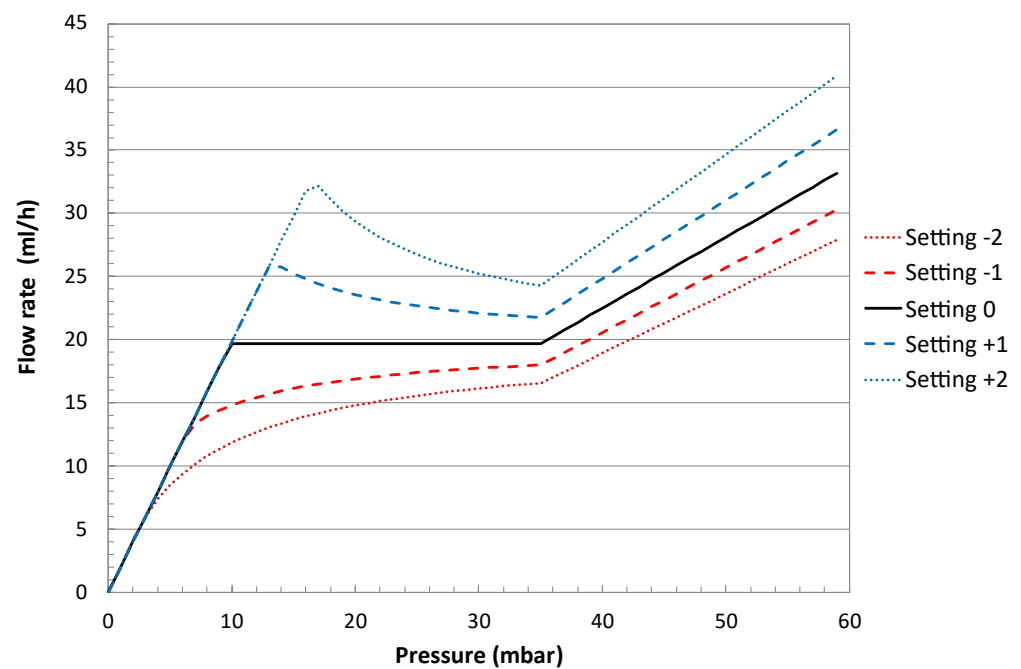


Figure 11. Simulated fluidic characteristics of a device described in [29] at five different settings corresponding to adjustment of the cylinder length from 13.5 mm to 15.5 mm using steps of 0.5 mm. The fluid medium is water at 37 °C.

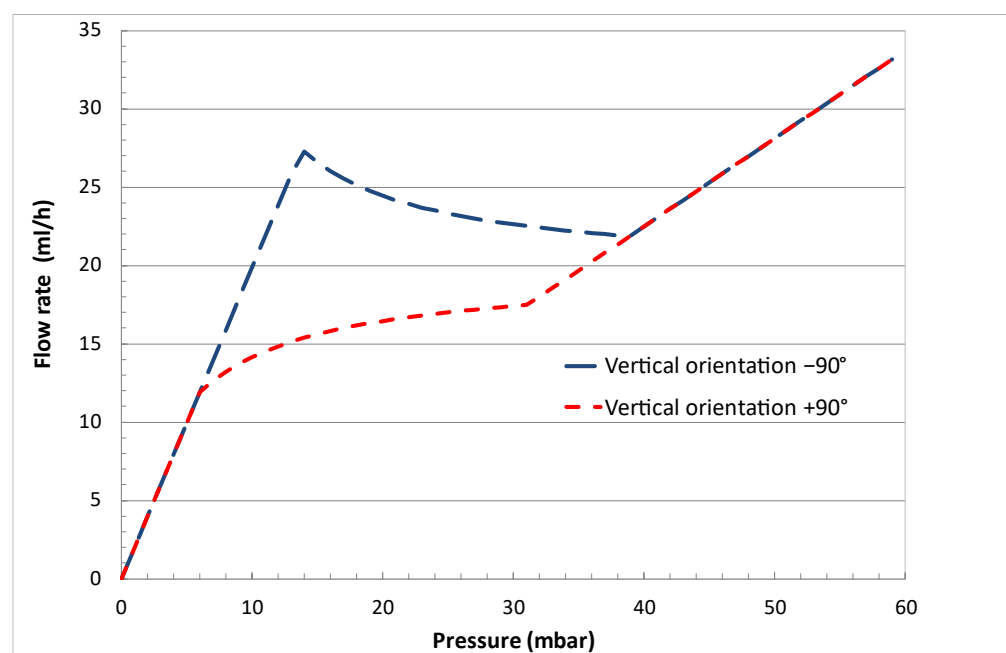


Figure 12. Simulated fluidic characteristics of a device described in [29] at two different vertical orientations (+90° with the inlet above the outlet and −90° with an outlet above the inlet). The fluid medium is water at 37 °C.

5. Conclusions

The nominal flow rate of a constant flow regulator is commonly set at the time of manufacture. However, an adjustment of this value by the end user could be desirable in several applications, including CSF drainage. Therefore, the adjustment of a flow regulator with a spring valve design was investigated here. A fluidic model was built, and a prototype was designed and tested at a constant temperature. The results show that the flow rate

can be adjusted up to at least $\pm 30\%$ from the nominal value by turning a flange a few mm. A numerical model was used to refine the design for CSF drainage application, specifically external ventricular drainage. This simple model offers the possibility to easily adjust a flow-regulated valve without the need for complex 3D FEM simulation tools with fluid-structure interactions. This feasibility study, which is a first attempt to realize the adjustability of a flow-regulated valve, opens new perspectives in the field of EVD and in any other application where the target flow rate is not known in advance. The next steps include fabrication and testing of devices dedicated to EVD, including evaluation of sensitivity to contaminants, self-cleaning and purge-mode capabilities, as well as usability testing for manual adjustment.

Funding: This research received no external funding.

Institutional Review Board Statement: Not applicable.

Informed Consent Statement: Not applicable.

Data Availability Statement: Not applicable.

Acknowledgments: Thanks to Ricardo Allendes for the mechanical drawings.

Conflicts of Interest: The author declares no conflict of interest.

Nomenclature

Symbol	Name
L_c	Cylinder length
L_p	Piston length
L_1	Inlet groove length
L_2	Outlet groove length
L_{reg}	Regulation length, with $L_c = L_1 + L_{reg} + L_2$
k	Spring stiffness
D_h	Hydraulic diameter of the channel
$2\pi b$	Helix pitch
L_{loop}	Length of one loop of the helicoidal channel
R	Piston radius
R_c	Cylinder radius
θ	Channel angle
η	Dynamic viscosity
L_{ch}	Active channel length
P	Applied pressure
S	Piston active surface
L_{min}	Minimum length of the piston engaged into the narrowest part of the cylinder
R_f	Fluidic resistance
$R_{f\ ch}$	Fluidic resistance of the channel
$R_{f\ losses}$	Parasitic fluidic resistance between the cylinder and piston
$R_{f\ line}$	Fluidic resistance of the fluidic line
ΔL	Piston displacement
P_{pret}	Minimum pressure to move the piston (pretension)
P_{th}	Minimum pressure to reach the piston mechanical stop
$L_{S\ free}$	Free length of the spring
$L_{S\ min}$	Minimum spring length
ΔL_{S0}	Initial spring compression length = $L_{S\ free} - (L_c - L_p)$
L_h	Piston recess
α	Channel length per unit of piston length = $L_{loop}/2\pi b$
β	Fluidic resistance of the channel per unit of channel length
φ	Device rotation angle
m	Piston effective weight
g	Gravitational acceleration

Abbreviation	Name
CSF	Cerebrospinal fluid
EVD	External Ventricular Drain
ICP	IntraCranial Pressure
MEMS	Microelectromechanical system
NPH	Normal-pressure hydrocephalus
PDMS	Poly(dimethylsiloxane)
PEEK	Polyether ether ketone

Appendix A. Mechanical Drawings of the Different Parts of the Adjustable Valve

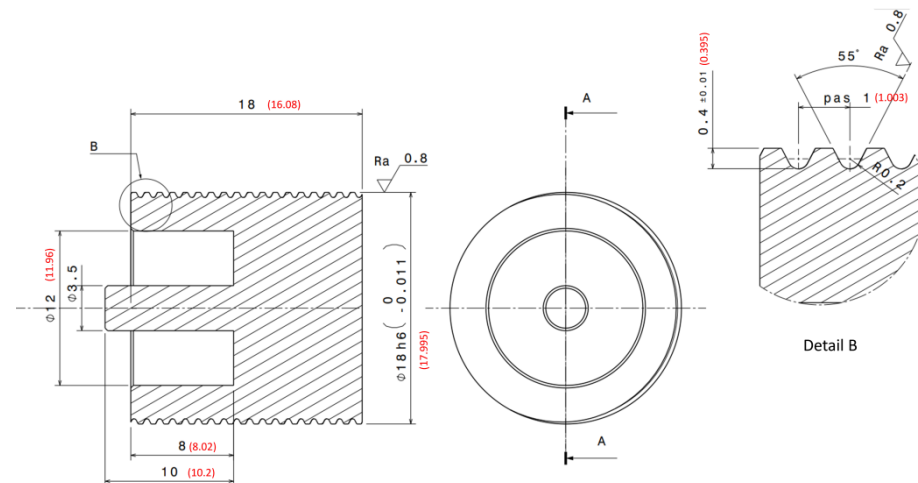


Figure A1. Mechanical drawing of the piston. Parentheses (red) indicate the measured dimensions of the sample.

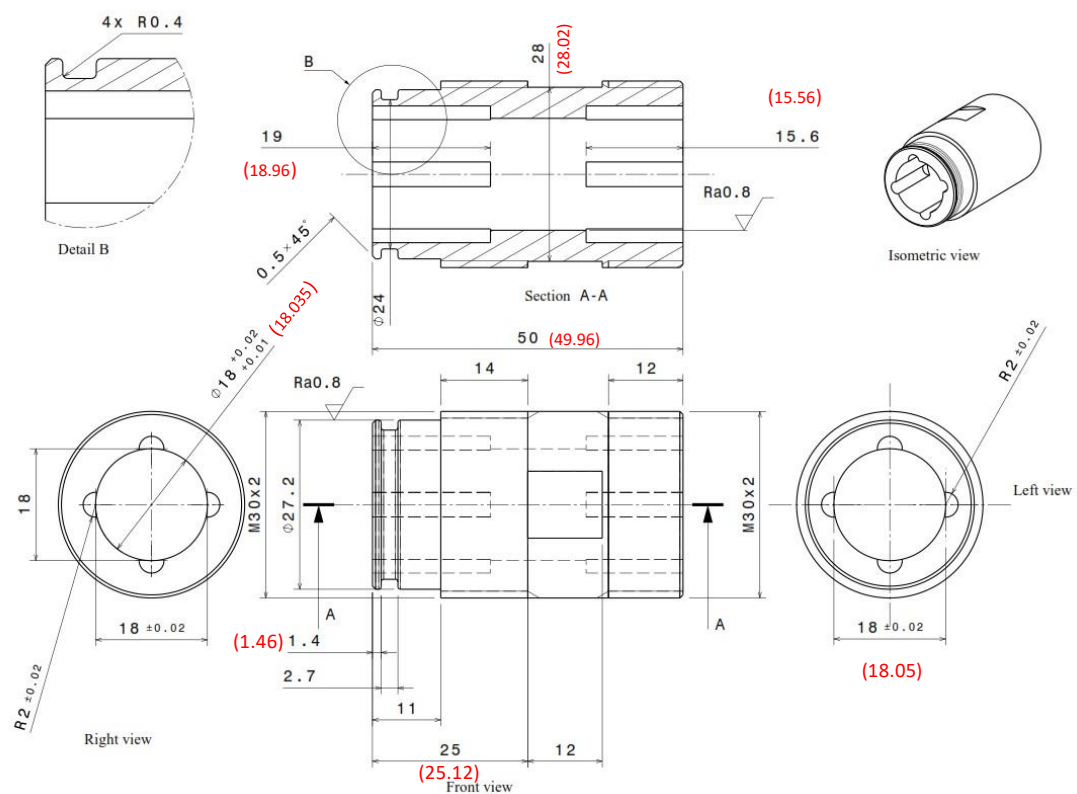


Figure A2. Mechanical drawing of the cylinder. Parentheses (red) indicate the measured dimensions of the sample.

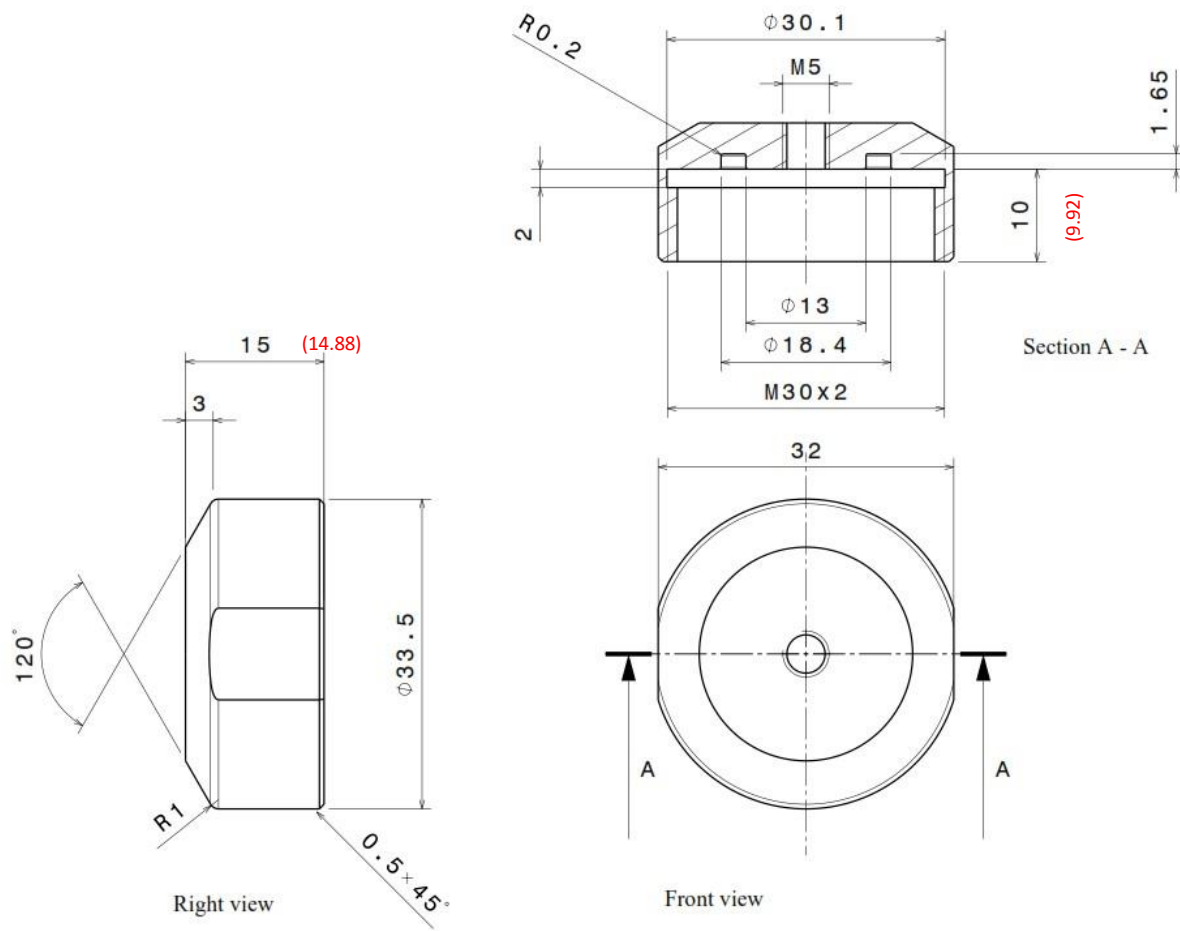


Figure A3. Mechanical drawing of the inlet flange. Parentheses (red) indicate the measured dimensions of the sample.

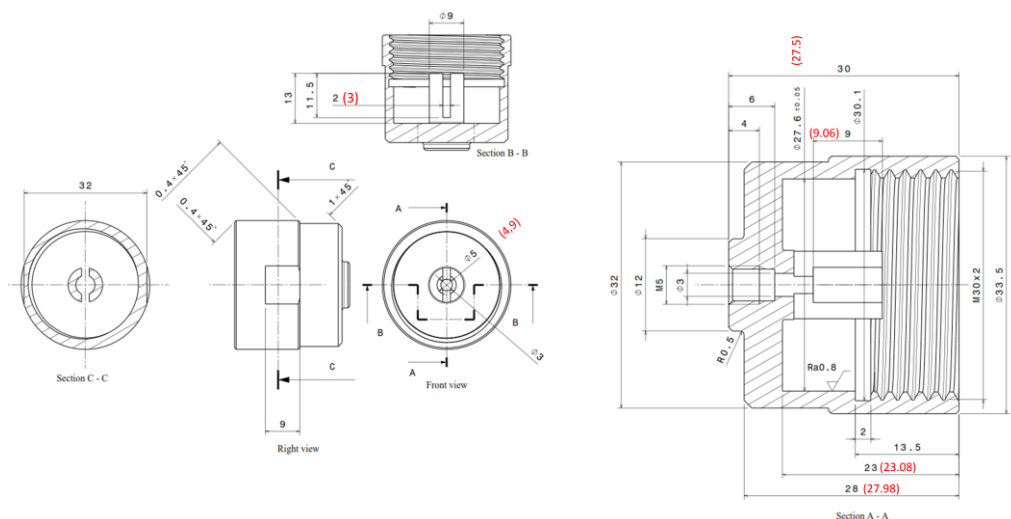


Figure A4. Mechanical drawing of the inlet flange. Parentheses (red) indicate the measured dimensions of the sample.

Appendix B. Spring Dimensions and Specifications

Material	Stainless Steel
Wire diameter	0.32 mm
External diameter	4.32 mm
Free length L_S free	41.9 mm
Min spring length L_{min}	10 mm
Max loaded length	9.68 mm
Solid length	6.9 mm
Spring stiffness k	0.0776 N/mm

References

- Chappel, E. A review of Passive Constant Flow Regulators for microfluidic applications. *Appl. Sci.* **2020**, *10*, 8858. [\[CrossRef\]](#)
- Warring, R.H. *Hydraulic Handbook*; Gulf Publishing Company: Houston, TX, USA, 1983; pp. 117–119.
- Cundiff, J.S. *Fluid Power Circuits and Controls: Fundamentals and Applications*; CRC Press: Boca Raton, FL, USA, 2001; pp. 140–143.
- Park, S.; Ko, W.; Prahl, J. A Constant Flow-Rate Microvalve Actuator Based on Silicon and Micromachining Technology. In Proceedings of the IEEE Technical Digest on Solid-State Sensor and Actuator Workshop, Hilton Head Island, SC, USA, 6–9 June 1988; pp. 136–139.
- Amacker, C.; Leung Ki, Y.-S.; Pasquier, V.; Madore, C.; Haller, M.; Renaud, P.; White, N. Passive Micro-Flow Regulator for Drug Delivery System. In Proceedings of the Eurosensors XII conference, Southampton, UK, 13–16 September 1998; pp. 591–594.
- Cousseau, P.; Hirschi, R.; Frehner, B.; Gamper, S.; Maillefer, D. Improved micro-flow regulator for drug delivery systems. In Proceedings of the 14th IEEE International Conference on Micro Electro Mechanical Systems MEMS 2001, Interlaken, Switzerland, 21–25 January 2001; pp. 527–530.
- Chappel, E.; Dumont-Fillon, D.; Mefti, S. 2014, March. Passive flow regulators for drug delivery and hydrocephalus treatment. In Proceedings of the Microfluidics, BioMEMS, and Medical Microsystems XII Conference, San Francisco, CA, USA, 1–6 February 2014; International Society for Optics and Photonics: Bellingham, WA, USA, 2014; Volume 8976, p. 89760S.
- Dumont-Fillon, D.; Hannebelle, M.; Van Lintel, H.; Chappel, E. Design of a passive flow regulator using a genetic algorithm. *Procedia Eng.* **2016**, *168*, 1016–1019. [\[CrossRef\]](#)
- Cornaggia, L.; Conti, L.; Hannebelle, M.; Gamper, S.; Dumont-Fillon, D.; Van Lintel, H.; Renaud, P.; Chappel, E. Passive flow control valve for protein delivery. *Cogent Eng.* **2017**, *4*, 1413923. [\[CrossRef\]](#)
- Conti, L.; Dumont-Fillon, D.; van Lintel, H.; Chappel, E. Silicon-to-silicon anodic bonding via intermediate borosilicate layer for passive flow control valves. *Int. J. Mech. Ind. Aerosp. Sci.* **2018**, *12*, 701–704.
- Chappel, E.; Musard, H.; Dumont-Fillon, D. Experimental Characterization and Modelling of Microfluidic Radial Diffusers for Passive Self-Regulating Valves. *Glob. J. Eng. Technol. Adv.* **2019**, *1*, 10–21. [\[CrossRef\]](#)
- Dumont-Fillon, D.; Lamaison, D.; Chappel, E. Design and Characterization of 3-Stack MEMS-Based Passive Flow Regulators for Implantable and Ambulatory Infusion Pumps. *J. Microelectromech. Syst.* **2020**, *29*, 170–181. [\[CrossRef\]](#)
- Tachatos, N.; Chappel, E.; Dumont-Fillon, D.; Meboldt, M.; Daners, M.S. Posture related in-vitro characterization of a flow regulated MEMS CSF valve. *Biomed. Microdevices* **2020**, *22*, 21. [\[CrossRef\]](#)
- Kartalov, E.P.; Walker, C.; Taylor, C.R.; Anderson, W.F.; Scherer, A. Microfluidic Vias Enable Nested Bioarrays and Autoregulatory Devices in Newtonian Fluids. *Proc. Natl. Acad. Sci. USA* **2006**, *103*, 12280–12284. [\[CrossRef\]](#) [\[PubMed\]](#)
- Liu, J.; Chen, Y.; Taylor, C.R.; Scherer, A.; Kartalov, E.P. Elastomeric Microfluidic Diode and Rectifier Work with Newtonian Fluids. *J. Appl. Phys.* **2009**, *106*, 114311. [\[CrossRef\]](#)
- Chang, H.-J.; Ye, W.; Kartalov, E.P. Quantitative Modeling of the Behaviour of Microfluidic Autoregulatory Devices. *Lab Chip* **2012**, *12*, 1890–1896. [\[CrossRef\]](#)
- Doh, I.; Cho, Y.H. Passive flow-rate regulators using pressure-dependent autonomous deflection of parallel membrane valves. *Lab Chip* **2009**, *9*, 2070–2075. [\[CrossRef\]](#)
- Zhang, X.; Xiang, N.; Tang, W.; Huang, D.; Wang, X.; Yi, H.; Ni, Z. A passive flow regulator with low threshold pressure for high-throughput inertial isolation of microbeads. *Lab Chip* **2015**, *15*, 3473–3480. [\[CrossRef\]](#) [\[PubMed\]](#)
- Zhang, X.; Wang, X.; Chen, K.; Cheng, J.; Xiang, N.; Ni, Z. Passive Flow Regulator for Precise High-Throughput Flow Rate Control in Microfluidic Environments. *RSC Adv.* **2016**, *6*, 31639–31646. [\[CrossRef\]](#)
- Zhang, X.; Zhu, Z.; Ni, Z.; Xiang, N.; Yi, H. Inexpensive, Rapid Fabrication of Polymer-Film Microfluidic Autoregulatory Valve for Disposable Microfluidics. *Biomed. Microdevices* **2017**, *19*, 21. [\[CrossRef\]](#)
- Zhang, X.; Zhang, Z. Microfluidic Passive Flow Regulatory Device with an Integrated Check Valve for Enhanced Flow Control. *Micromachines* **2019**, *10*, 653. [\[CrossRef\]](#)
- Chari, A.; Czosnyka, M.; Richards, H.K.; Pickard, J.D.; Czosnyka, Z.H. Hydrocephalus shunt technology: 20 years of experience from the Cambridge Shunt Evaluation Laboratory. *J. Neurosurg.* **2014**, *120*, 697–707. [\[CrossRef\]](#)

23. Codman Specialty Surgical. *Flow Regulating Valves*; 1100665-1-EN; Integra LifeSciences Corporation: Princeton, NJ, USA, 2018.
24. Paes, N.A. New Self-Adjusting Flow-Regulating Device for Shunting of CSF. *Childs Nerv. Syst.* **1996**, *12*, 619–625. [[CrossRef](#)]
25. Yang, B.; Levis, J.W.; Lin, Q. A PDMS-Based Constant-Flowrate Microfluidic Control Device. In Proceedings of the 17th IEEE International Conference on Micro Electro Mechanical Systems. Maastricht MEMS 2004 Technical Digest, Maastricht, The Netherlands, 25–29 January 2004; pp. 379–382.
26. Yang, B.; Lin, Q. Planar Micro-Check Valves Exploiting Large Polymer Compliance. *Sens. Actuator A Phys.* **2007**, *134*, 186–193. [[CrossRef](#)]
27. Yang, B.; Lin, Q. A Planar Compliance-Based Self-Adaptive Microfluidic Variable Resistor. *J. Microelectromech. Syst.* **2007**, *16*, 411–419. [[CrossRef](#)]
28. Zhang, Q.; Peng, X.; Weng, S.; Zhang, R.; Fang, D.; Zhao, R.; Qi, H.J. Self-Adaptive Flexible Valve as Passive Flow Regulator. *Extreme Mech. Lett.* **2020**, *39*, 100824. [[CrossRef](#)]
29. Chappel, E. Design and characterization of a passive flow control valve dedicated to the hydrocephalus treatment. *Cogent Eng.* **2016**, *3*, 1247612. [[CrossRef](#)]
30. Su, Q.; Chen, W.; Chen, W.; Jin, Z.; Lin, Z. Flow Regulation Performance Analysis of Microfluidic Passive Valve for High Throughput Liquid Delivery. *Micromachines* **2022**, *13*, 687. [[CrossRef](#)] [[PubMed](#)]
31. Sainte-Rose, C.; Hooven, M.D.; Hirsch, J.-F. A New Approach in the Treatment of Hydrocephalus. *J. Neurosurg.* **1987**, *66*, 213–226. [[CrossRef](#)] [[PubMed](#)]
32. Chappel, E.; Hannebelle, M.; Cornaggia, L.; Dumont-Fillon, D.; Momjian, S. Hybrid hydrodynamic characteristic for hydrocephalus valve: A numerical investigation using electrical equivalent networks. *Cogent Eng.* **2017**, *4*, 1415103. [[CrossRef](#)]
33. Chappel, E. Method of Adjustment for Hydrocephalus Valve. U.S. Patent N° 2017203083(A1), 20 July 2017.
34. Czosnyka, M.; Czosnyka, Z.; Whitehouse, H.; Pickard, J.D. Hydrodynamic properties of hydrocephalus shunts: United Kingdom shunt evaluation laboratory. *J. Neurol. Neurosurg. Psychiatry* **1997**, *62*, 43–50. [[CrossRef](#)] [[PubMed](#)]
35. Chung, D.Y.; Olson, D.M.; John, S.; Mohamed, W.; Kumar, M.A.; Thompson, B.B.; Rordorf, G.A. Evidence-Based Management of External Ventricular Drains. *Curr. Neurol. Neurosci. Rep.* **2019**, *19*, 94. [[CrossRef](#)] [[PubMed](#)]
36. Chappel, E. Adjustable Passive Flow Regulator. European Patent N° EP2943708B1, 6 September 2017.
37. Chappel, E. (Ed.) *Drug Delivery Devices and Therapeutic Systems*; Academic Press: New York, NY, USA, 2020.
38. White, F.M. *Viscous Fluid Flow*, 2nd ed.; McGraw-Hill: New York, NY, USA, 1991.

Disclaimer/Publisher’s Note: The statements, opinions and data contained in all publications are solely those of the individual author(s) and contributor(s) and not of MDPI and/or the editor(s). MDPI and/or the editor(s) disclaim responsibility for any injury to people or property resulting from any ideas, methods, instructions or products referred to in the content.